# CHAPTER 5

## Synthesis of fluorescent carbon quantum dots from *Jatropha* fruits and their application in fluorometric sensor for the detection of chlorpyrifos

## 5.1. Introduction

Organophosphates (OPs) are one of the most important pesticides which have been extensively used in agriculture to prevent insect eradication across the world, resulting into the increment of the productivity of crops and vegetables [K.Liu *et al.* (2016), J.Pretty *et al.* (2008)]. According to World Health Organization (WHO), 1.5 billion incidents of diarrhea in children, lead to more than 3 million death reports in each year caused by the contamination of OPs in food, air, water, as well as agricultural products. However, the lower concentration of OPs causes several problems in the human body such as the nervous system, cardiovascular system and also affects the respiratory system [N. Zhang *et al.* (2014), Z. Zheng *et al.* (2011), Z. Li *et al.* (2014)]. Among OPs, chlorpyrifos (Cpf) is a man-made organophosphate insecticide which plays an important role in the field of agriculture. It is commonly used to control the insects that attack on fruits, vegetables, landscaping plants, and so on. However, excess Cpf concentration has deleterious effects on the environment and causes several diseases in human beings such as carcinogenicity, neurotoxicity, mutagenic and endocrine disruption [S.A. Nsibande *et al.* (2016), M.A. Kamyabi *et al.* (2020), S. Islam *et al.* (2019), Y. He *et al.* 2019)]. Therefore, it is a very urgent demand to develop a fast, rapid, sensitive, and reliable technique for the accurate diagnosis of Cpf detection to improve food safety as well as ecosystem protection [P. Wang *et al.* (2013), D. Ayodhya *et al.* (2019), Y.A. Kim *et al.* (2011)]. To date, various analytical approaches and instrumental techniques have been established for the determination of OPs in food and water. For instance, mass spectroscopy, [J. Lee *et al.* (2011)] gas chromatography (GC), [E. Johannesen *et al.* (2007), T.A. Albanis *et al.* (2004)] high-performance liquid chromatography (HPLC), [C.C. Leandro *et al.* (2006), C. Padrón Sanz *et al.* (2004)] enzyme-linked immunosorbent test, [J.A.

Gabaldón *et al.* (2007)] and electrochemical assay [A. Chen *et al.* (2012), Y. Wang *et al.* (2011), D. Du *et al.* (2012), S. Viswanathan *et al.* (2009)] have been accomplished for the detection of OPs. Unfortunately, these techniques are based on time consumption, sophisticated instrumentation, complex sample preparation, and require trained operators. [Q. Long *et al.* (2015)] Thus, these conventional methods are not appropriate for practical applications. Therefore, to overcome these problems, the development of an innovative sensing probe is still a challenging task.

In recent times, the optical techniques such as absorption and fluorescence spectroscopy has attracted much attention for the detection of OPs owing to their good sensitivity, selectivity, effective simplicity, short-time response, and low cost [J. Hou *et al.* (2015), M. Liang *et al.* (2013), N. Fahimi-Kashani *et al.* (2016)]. In previous studies, many of the research groups have reported nanomaterials for the determination of OPs through fluorometric and colorimetric counting gold, Cd, oxide-based nanomaterials, carbon nanotubes, graphene quantum dots, and so on. For instance, Jiang *et al.* have synthesized a rhodamine B-covered gold nanoparticle (RB-AuNPs) probe for the detection of OPs over fluorometric and colorimetric procedures [D. Liu *et al.* (2012). Sun et al. has reported the Cd-Te QDs and AuNPs probes for the turn-on fluorescence detection of glyphosate [J. Guo *et al.* (2014)]. Xie *et al.* has developed lipoic acid capped AuNPs based on colorimetric detection of highly toxic OPs and nerve agents [J. Sun *et al*. (2011)] However, these nanomaterial-based probes have been synthesized via expensive chemicals and complicated synthesis procedures, which may exhibit adverse effects on human health and the environment.

Now days, the fluorescence-based Carbon Quantum dots (CQDs) have much potential to be designed as a novel sensing probe for the investigation of OPs. Recently, the fluorescent carbon quantum dots have excellent properties such as easy preparation, commercial availability, high water solubility, low cytotoxicity, and eco-friendly [Y. Wan *et al.* (2019), X. Wu *et al.* (2017)]. The tremendous applications of CQDs are widely used in several fields, including cell imaging, sensors, drug delivery, LED devices, photocatalysis and so on. Moreover heavy metal toxicity and expensive as well as corrosive chemical synthesis route adopted for the synthesis of quantum dots could be the biggest challenges for their successful biological and environmental benign application. During the synthesis process, we tried to synthesized carbon quantum dots from other plant sources, but the quantum yield and fluorescence were very low compared to Jatropha fruits which is abundantly available in BHU campus. Most importantly the targeted application of this research supported from the fact that Jatropha plants being successful enough to deal with environmental pollution caused by pesticides [K. Bauddh *et al.* (2017), F.O. Okeola *et al.* (2017), R. Kamusoko *et al.* (2017)]. So, we have chosen Jatropha Fruits for the detection of chlorpyrifos due to its low cost, abundant availability and potency.

Here, we have designed the fluorescent nanoprobe by using J-CQDs for the detection of OPs based on the catalytic reaction of Acetylcholinesterase (AChE). The OPs compounds irreversibly inhibit the activity of AChE [H. Li *et al.* (2017), X. Yan *et al.* (2015) H. Li *et al.* (2018), K. Zhang *et al.* (2010) Reshma *et al.* (2010) J. Lintelmann *et al.* (2003)]. The inhibition of AChE activity permits acetylcholine to stay active in the synapse, thus leading to the deadly consequences [T.R. Fukuto *et al.* (1990), J.S. Van Dyk *et al.* (2011) D.M. Klotz *et al.* (1997). It is found that, the neurotransmitter acetylcholine (ATCh) is catalyzed into

thiocholine (TCh) by the use of AChE present in humans. Further, TCh activates the decomposition of Ellman's reagent 5,5-dithiobis (2-nitrobenzoic acid) (DTNB) into specific yellow-colored 5-thio-2-nitrobenzoic acid (TNBA) [X. Meng *et al.* (2015), J. Dong *et al.* (2013), M. Moser *et al.* (2016)]. The produced TNBA efficiently quenches the fluorescence of J-CQDs. Thus, in this study, we have designed the fluorescence nanoprobe for the detection of Cpf based on inhibition of AChE enzyme activity.

## 5.2. Materials and method

### 5.2.1. Synthesis of CQDs

The fruits of Jatropha were rinsed systematically with ultrapure distilled water and chopped into the small pieces. An appropriate amount (150 g) of chopped fruits were dissolved in 200 mL of distilled water in the beaker and transferred to 250 mL Teflon-lined autoclave. The autoclave was tightly sealed and kept for 5 hours at $180^0$C in a hot air oven. After carbonization, the furnace was allowed to cool down naturally to room temperature. The obtained dark brownish solution was centrifuged at 10000 rpm for 25 minutes to eliminate the larger particles. Then the supernatant part was passed through a 0.22 µm filtration membrane to remove larger particles and impurities. Finally, the synthesized fluorescent J-CQDs solution was dispersed in double distilled water at a concentration 4 µg/mL and then preserved at 4 ºC for further study. The schematic representation of synthesized J-CQDs is shown below**.**

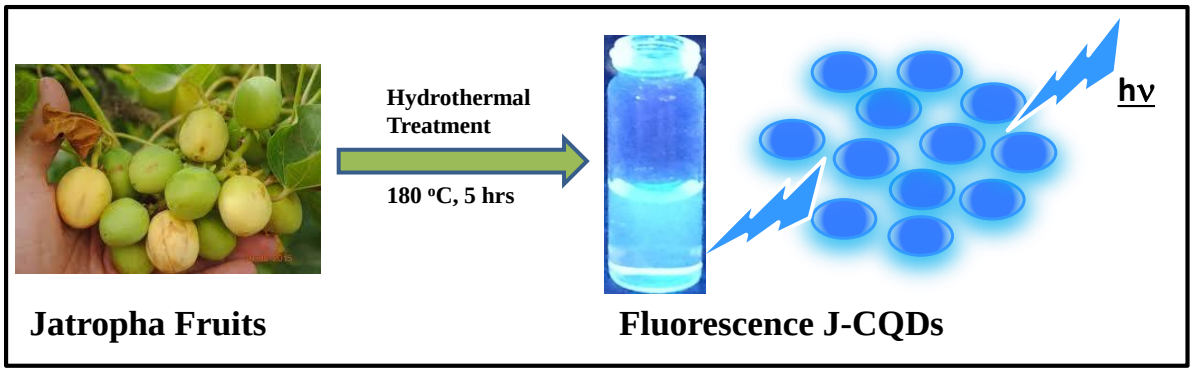


**Scheme 5.1.** Illustration of the one-step synthesis of J-CQDs from the Jatropha fruits.

### 5.2.2. Assay for AChE activity

In a typical assay, a series of different concentrations of AChE (50 µL) ranging from 0 to 100 mU/mL were added with substrate ATCh (50 µL, 10 mmol/L) in 1.0 mL of Tris-HCl buffer (10 mmol/L, pH 7). After incubating at $37^0$C for 25 minutes, 50 µL of as-prepared J-CQDs and DTNB (50 µL, 200 µg/mL) were added. Then, the above reaction mixture was diluted to 500 µL double-distilled water and shaken thoroughly for 5.0 minutes. After that, the mixed solution was transferred into 1 cm quartz cuvette, thereafter, absorption and fluorescence spectra were recorded.

### 5.2.3 Detection of chlorpyrifos

In a typical enzyme inhibition assay, the different concentrations of Cpf (100 µL) were added to the AChE solution (80 mU/mL, 50 µL) under 37 °C for 30 min. Then, ATCh (50 µL, 10 mmol/L) and Tris-HCl buffer (1.0 mL of 10 mmol/L) at pH 7 were successively introduced into the system. After incubating at 37 °C for 25 min, DTNB (50 µL, 200 µg/mL) and J-CQDs (50 µL) along with double-distilled water (500 µL) were added and mixed thoroughly for 5.0 min at room temperature. The absorbance and fluorescence spectra of the above

reaction system/mixture were recorded with the help of spectrophotometer and flurometer respectively.

### 5.2.4 Experimental methodology

The prepared fluorescent J-CQDs were characterized through the various spectroscopic and micrographic techniques. The UV-visible absorbance spectra were scanned using Thermo Scientific, Evolution 201 spectrophotometer. XRD spectra were traced by using Rigaku MiniFlex 600. The shape and size were probed via TEM, TECHNAI $G^2$ 20 S-TWIN. The chemical composition and bond present were identified by XPS, AMICUS. The FTIR spectra were obtained by Perkin Elmer Spectrum 100. The fluorescence spectra were conducted by PTI QM-8000 Series fluorescence spectrophotometer. The time resolve fluorescence spectra were conducted by Edinburgh Instrument and the zeta potential were performed on the Nano Zeta Sizer Malvern apparatus.

### 5.2.5. Quantum yield determination

The quantum yield of the synthesized CQDs was measured in reference to quinine sulphate from the given **equation 2.1** mentioned in **chapter 2** in a **section 2.6.1**.

## 5.3. Results and discussion

### 5.3.1. Characterizations

The prepared J-CQDs were characterized by TEM analysis for the morphology and size distribution. **Figure 5.1a** shows the representative TEM image of J-CQDs, which exhibited a narrow size distribution around 1.8-4.8 nm with an average size of 3.2 nm **(Figure 5.1b).** The particles were calculated by imageJ software. The hydrodynamic size of the synthesized J-CQDs was 37.8 nm, as shown in **Figure 5.2**. These results confirmed that formed J-CQDs

were mostly spherical in shape and well dispersed. The typical SAED micrograph **(Inset in Figure 5.1a)** represents a broad circular ring for the amorphous nature of prepared J-CQDs. From the XRD **(Figure 5.1c)** pattern of J-CQDs, which exhibited the broad peak at $2\theta=24.6^{o}$ along with the reflection of (002) [D. Bano *et al.* (2018)], which resembles to the amorphous and graphitic structure. The functional moieties existing on the surface of J-CQDs were characterized through FT-IR spectra, this results displayed characteristic functional groups on surface, such as the peak at 3404 $cm^{-1}$ ($\nu_s$ = -OH), 2934 $cm^{-1}$ ($\nu_s$ = -C-H), 1614 $cm^{-1}$ ($\nu_s$ =C-H), 1398 $cm^{-1}$ ($\nu_s$ = -C=C), 1082 $cm^{-1}$ ($\nu_s$ = -C-O-C) and 625 $cm^{-1}$ ($\nu_s$ = -C-H bending), as shown in **Figure 5.1d** [J. Yu *et al.* (2016), A. Zhu *et al.* (2012)].

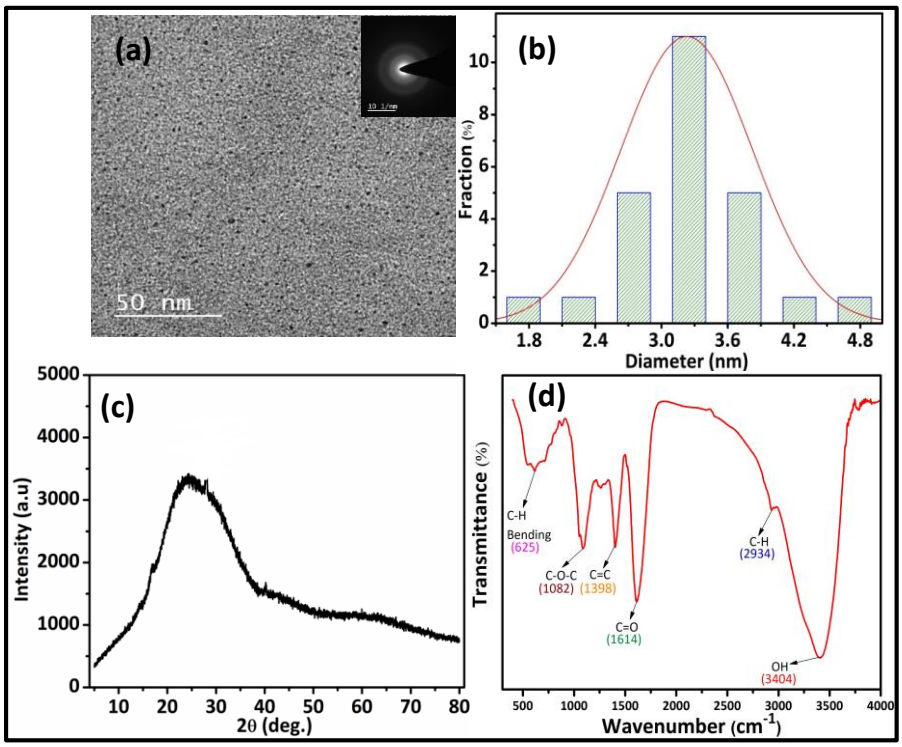


**Figure 5.1.** (a) TEM micrograph of synthesized J-CQDs with insect SAED image. (b) average size distribution histogram. (c) P-XRD pattern and (d) FT-IR spectrum of J-CQDs.

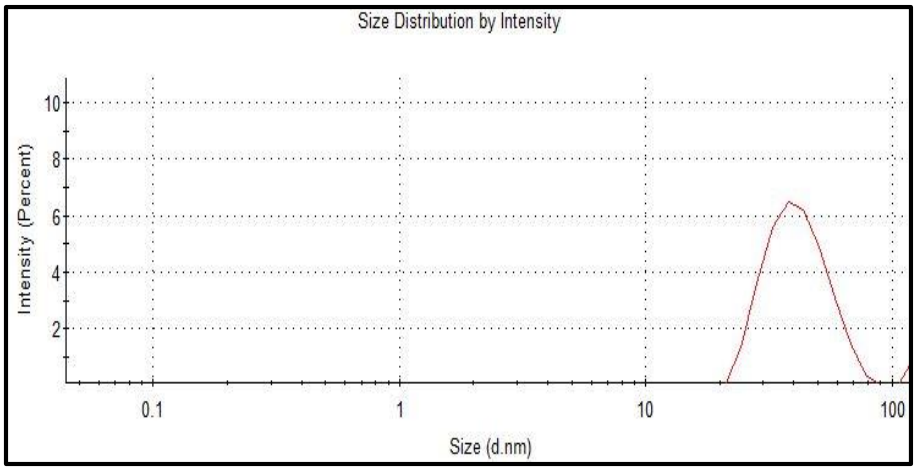


**Figure 5.2** The hydrodynamic size of as-synthesized J-CQDs.

XPS analysis was carried out to determine the elemental composition on the surface and the chemical state of J-CQDs as displayed in **Figure 5.3**. The wide range XPS spectrum of as-prepared J-CQDs shows the characteristic peaks corresponding to C, N, and O at 284.28 eV, 398.45 eV, and 531.02 eV, respectively, as depicted in **Figure 5.3a.** It can be found that the as-synthesized J-CQDs were mainly composed of C, N, and O. As presented in **Figure 5.3b,** the high-resolution spectra of C1s exhibited five peaks at 283.10 eV, 284.36 eV, 284.95 eV, 285.58 eV and 286.39 eV, which are assigned to the C=C, C-C, C-O, C=N, and C=O bonds respectively[48]. As shown in **Figure 5.3c,** the N1s spectrum deconvoluted into three peaks at 397.65 eV, 398.21 eV, and 398.71 eV corresponds to the presence of Pyridinic N, -C-N-C, and Pyrrolic N moieties, respectively. As shown in **Figure 5.3d,** the high resolution of the O1s spectrum mainly consisted four peaks at 530.47 eV, 531.02 eV, 531.52 eV, and 532.50 eV, which are credited to the presence of C-O-H, C-O-C, C=O, and C-O bonds, respectively.

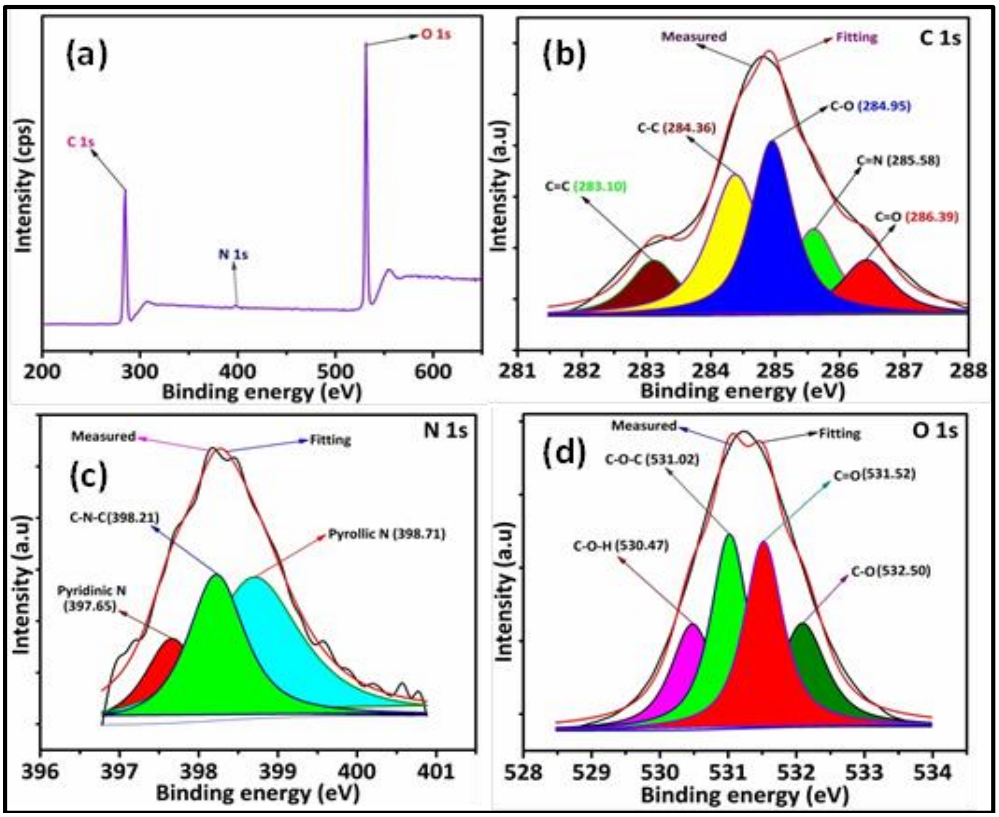


**Figure 5.3** (a) XPS spectra of J-CQDs, wide range spectra (b) C1s (c) N1s and (d) O1s spectra

### 5.3.2. Optical Properties

The photo-physical properties of as-prepared J-CQDs were investigated in an aqueous solution through fluorescence and UV-visible absorption spectroscopy, as shown in **Figure 5.4.** The aqueous solution of J-CQDs exhibited bright blue fluorescence under excitation of 365 nm in a UV chamber. These results verify that the synthesized J-CQDs are fluorescent in nature. It can be seen that the single absorption band of aqueous solution showed at 265 nm, which ascribed to the $\pi$–$\pi^*$ electronic transition of C=C bond **(Figure 5.4a)**, [X. Zhu *et al.* (2014)] and the maximum emission was observed at 462 nm at the excitation wavelength of 370 nm.

Interestingly, the fluorescence emission spectra were measured at different excitation wavelengths from 300 nm to 510 nm at 10 nm intervals, as shown in **Figure 5.4b.** Initially, the excitation wavelength increased from 300 nm to 510 nm, and the emission intensity gradually increased with a bathochromic shift. Upon further, the excitation wavelength increased from 380 nm to 510 nm, and then the emission intensity progressively decreased. Thus, this result confirmed that the excitation-dependent emission behavior arises due to the presence of different trap surface states in J-CQDs [Y. Hu *et al.* (2017)]. The as-prepared J-CQDs exhibited a good fluorescence quantum yield around 13.7 % under the excitation 360 nm using quinine sulfate (54% in 0.1 M $H_2SO_4$) as a reference. The high quantum yield may have been resulted from the different functional groups on the surface of the J-CQDs. The excellent photophysical properties, high emission quantum yield, and size-tunable emission of as-synthesized J-CQDs have become one of the most fluorescent nanomaterials for potential applications in sensing. As shown in **Figure 5.4c**, the CIE coordination in a highly blue region at (0.16, 0.17) confirmed the blue color emission of as-synthesized J-CQDs. The fluorescence intensity of the J-CQDs was explored at different pH from 2-12 to observe the effect of pH. As shown in **Figure 5.4d**, negligible change in fluorescence spectra was observed up to pH 8, while above this pH fluorescence quenching was observed. In highly basic medium, the protonation of carboxylic group on the surface of J-CQDs cause aggregation, which results to the fluorescence quenching [Y. Song *et al.* (2014)]. This outcome suggested that the J-CQDs could be used in a wide pH range from 2 to 8.

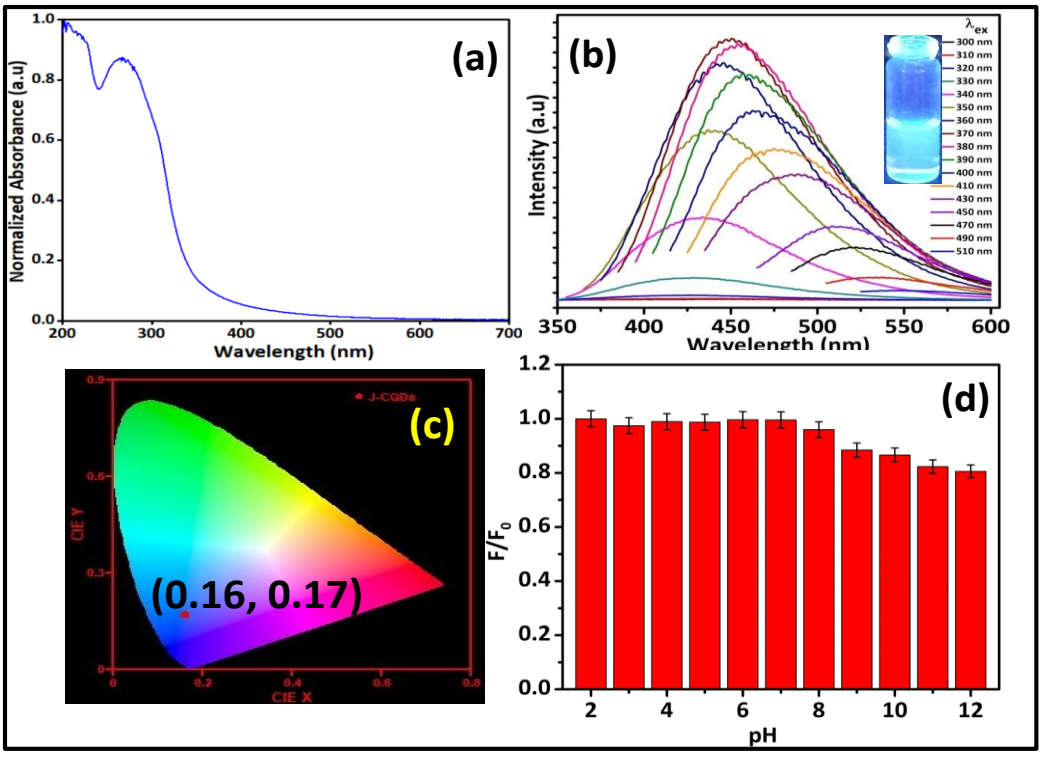


**Figure 5.4** (a) UV-visible absorption spectrum and (b) different excitation (300- 510 nm) dependent emission spectrum of synthesized J-CQDs. (c) CIE color Co-ordinate (0.16, 0.17) diagram of J-CQDs is showing blue color (d) Effect of different pH, on the emission of J-CQDs

Moreover, the stability of the synthesized J-CQDs was also investigated under the high salt concentration. As shown in **Figure 5.5**, an insignificant change in fluorescence emission intensity was observed on the addition of different NaCl concentrations from 1 to 10 M.

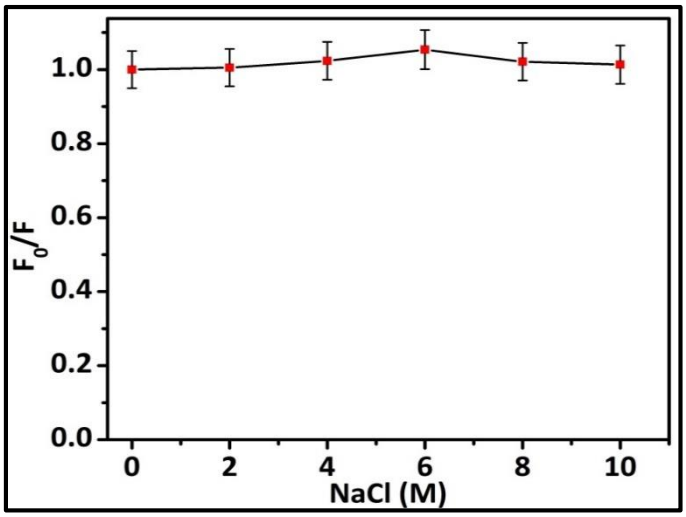


**Figure 5.5** Effect of emission spectra of J-CQDs on adding different NaCl concentration.

This result confirms that the synthesized J-CQDs resist the high ionic strength conditions. Moreover, stability of synthesized J-CQDs was checked over 8 months; no apparent loss of fluorescence emission suggested the synthesized J-CQDs have long durability, as shown in **Figure 5.6.**

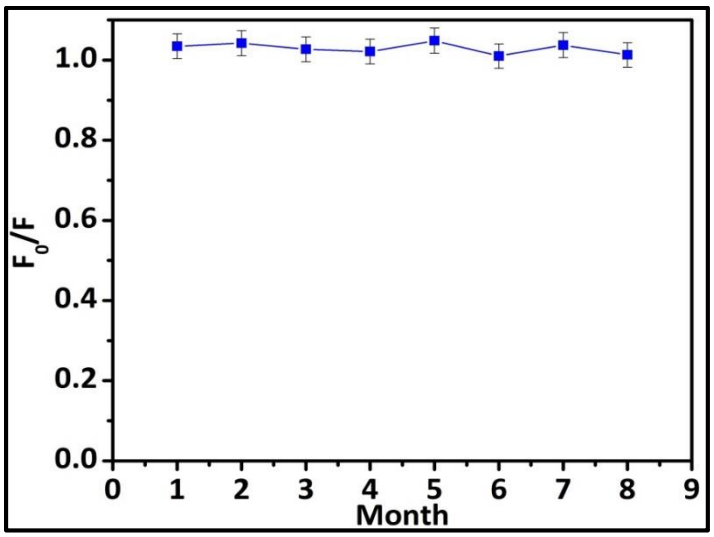


**Figure 5.6** Effect of fluorescence intensity after 8 months of incubation at 5 $^{o}$C.

### 5.3.3. Detection assay of chlorpyrifos

The detection strategy of OPs depends on the AChE, which catalyzes the hydrolysis of ATCh into thiocholine (TCh). As shown in **Figure 5.7a**, no visible change in absorbance spectra was observed in case of J-CQDs + DTNB (black line), J-CQDs + DTNB + ATCh (red line) and J-CQDs + DTNB + ATCh + AChE + Cpf (pink line) reaction systems. However, the apparent yellow color was observed for the reaction system of J-CQDs + DTNB + ATCh + AChE (blue line) along with a characteristic absorption peak at 412 nm. Thus, AChE catalyzed the reaction system and produced TCh. In the proposed reaction system, TCh decomposed the DTNB into yellow color TNBA, as shown in **equation 1**.

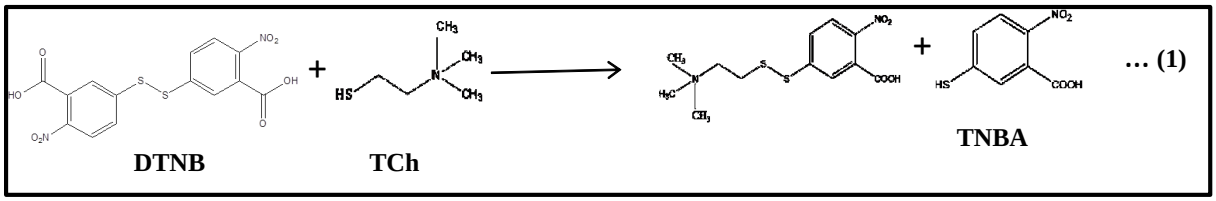


Further, the fluorescence intensity of the above reaction system was also examined. Remarkable fluorescence change was observed in reaction system of J-CQDs + DTNB + ATCh + AChE, while insignificant change was observed for the rest of the proposed reaction system, as shown in **Figure 5.7b**. Hence, we can conclude from the UV-visible and fluorescence data that the AChE hydrolyzed ATCh into TCh, thus, TCh triggered DTNB into yellow colored TNBA.

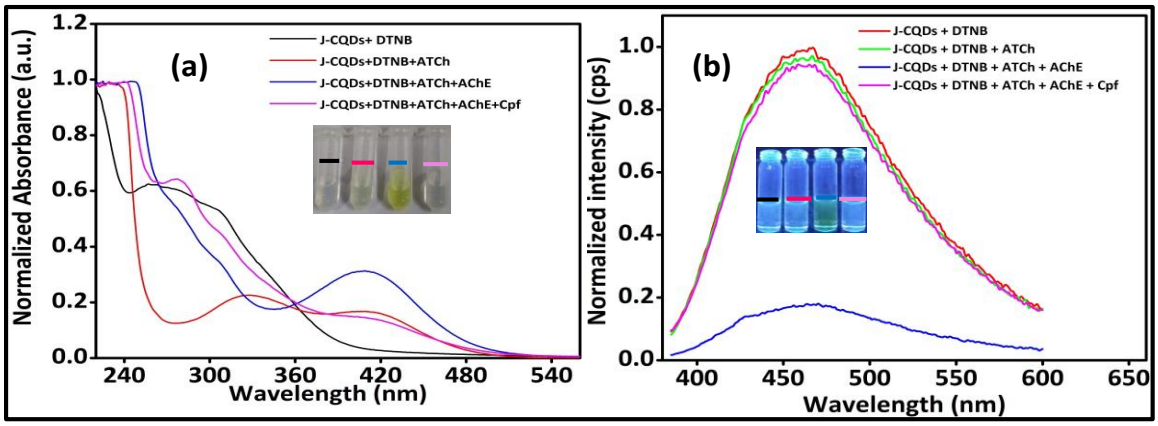


**Figure 5.7** (a) UV-visible spectrum of J-CQDs+DTNB, J-CQDs+DTNB+ATCh, J-CQDs+DTNB+ATCh+ AChE and J-CQDs+DTNB+ATCh+AChE+Cpf system (b) fluorescence spectrum.

Moreover, the fluorescence emission spectra of J-CQDs + DTNB + ATCh were observed as a function of AChE concentration. The fluorescence intensity decreased gradually with the increasing concentration of AChE from 0 to 100 mU/mL,as shown in **Figure 5.8a**. A good linear plot was observed in between 30 and 80 mU/mL along with $R^2$ is equal to 0.995, as shown in **Figure 5.8b.** Therefore, to pursue high sensitivity, 80 mU/mL of AChE was selected to further study.

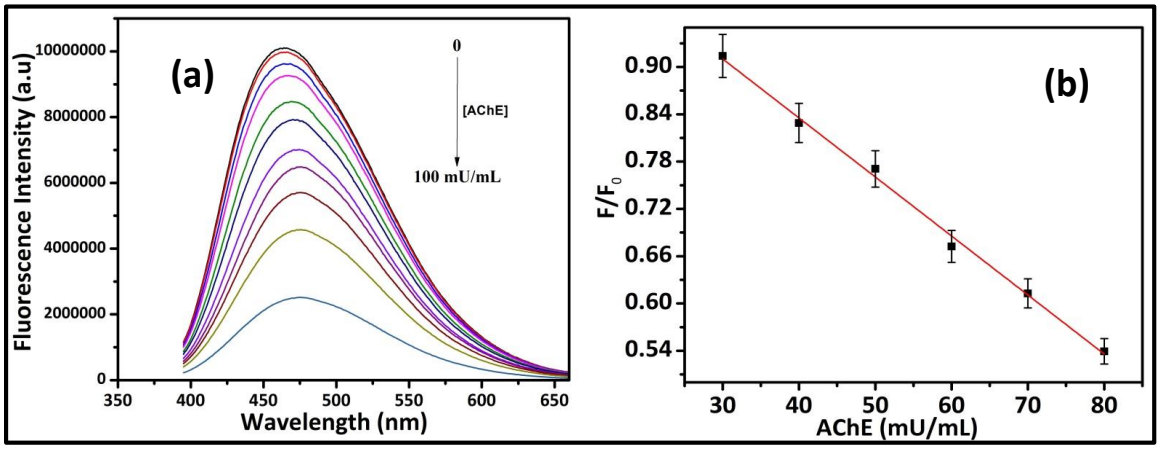


**Figure 5.8 (a)** Represents the emission intensity of ATCh + J-CQDs + DTNB system on varying AChE concentration from 0 to 100 mU/mL, **(b)** corresponding fluorescence change in a linear range of 30-80 mU/mL.

The effect of different concentration of ATCh (0.1–1.0 mol/L), AChE (20–120 mU/mL), DTNB (0.1–1.0 mol/L) and Cpf (2–12 μg/ mL) on the emission intensity of J-CQDs were investigated, individually. As displayed the negligible change in fluorescence emission of J-CQDs in presence of ATCh **(Figure 5.9a)**, AChE **(Figure 5.9b)**, DTNB **(Figure 5.9c)** and Cpf **(Figure 5.9d)** indicates the feasibility of designed nano-probe based on AChE.

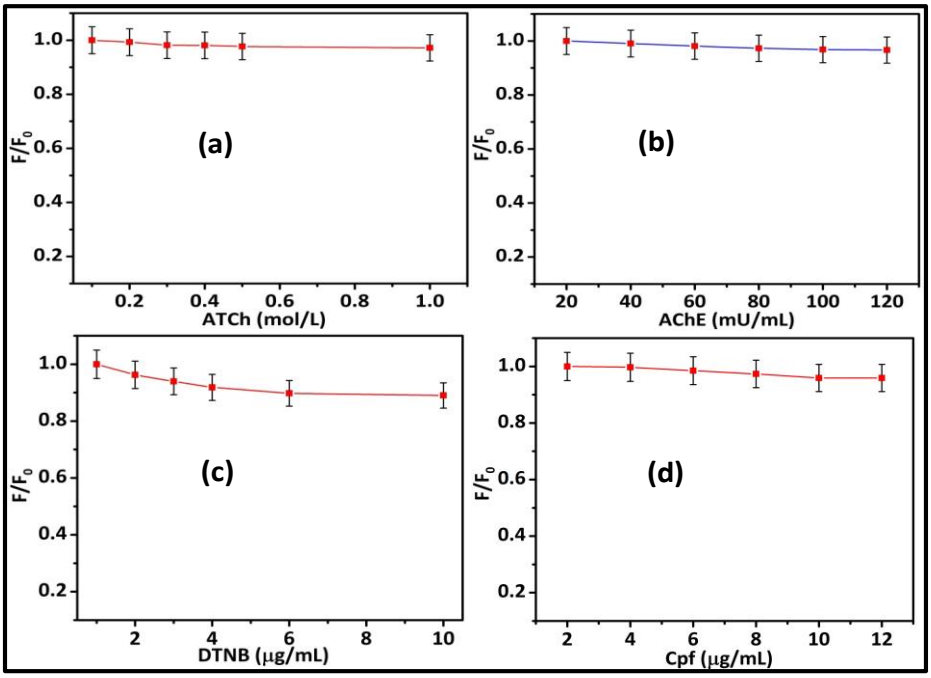


**Figure 5.9** Influence of (a) ATCh, [0.1–1.0 mol/L] (b) AChE, [20–120 mU/mL] (c) DTNB [0.1–1.0 mol/L] and (d) Cpf [2–12 μg/ mL] on emission intensity of J- CQDs [4 μg/mL]

To design the fluorescence based nano-probe, the different parameters were optimized such as pH, temperature, and reaction time, which may influence the sensing system. These optimum parameters have been thoroughly analyzed with the help of a fluorescence spectrophotometer. The inhibition efficiency (IE) of AchE by OPs was measured with the given formula.

$$IE = (I_{inhibitor} - I_{no\ inhibitor}) / (I_0 - I_{no\ inhibitor}) \quad ...(2)$$

Where $I_{inhibitor}$ and $I_{no\text{-}inhbitor}$ represents to the emission intensity of J-CQDs/DNTB/ATCh/AChE/Cpf system and J-CQDs/DNTB/ATCh/AChE system, respectively. $I_0$ represents emission intensity of the J-CQDs/DNTB/ATCh system.

Firstly, the influence of different pH (2-12) was investigated in presence of Cpf in the reaction system of J-CQDs + DTNB + ATCh + AChE. The maximum IE of AChE was found at pH 7, as shown in **Figure 5.10a**. The incubation time of Cpf and AChE was further explored at different time intervals, as shown in **Figure 5.10b**. This result revealed that the 25 minutes is enough to complete inhibition. Besides, the effect of temperature on IE of Cpf was also probed, as shown in **Figure 5.10c**. The maximum IE was found at 37 °C. Thus, the optimum parameter for detection of Cpf was established at pH 7, 25 min of reaction time and temperature 37° C.

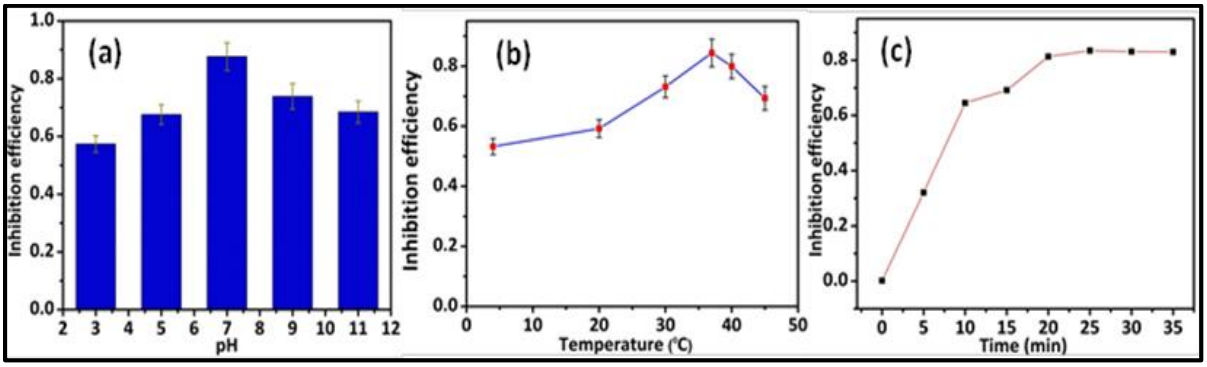


**Figure 5.10.** Influence of Cpf concentration on IE of reaction system J-CQDs + DTNB + ATCh + AChE at (a) different pH [2-12], (b) different temperature, and (c) different incubation time; [Cpf = 0.2 μg/mL].

### 5.3.4. Detection of chlorpyrifos

To this experiment, the fluorescence mode was observed in order to probe the Cpf. On increasing the concentration of Cpf from 0.0 to 1.0 μg/mL, the fluorescence intensity of JQDs + ATCh + AChE + DTNB increases, as shown in **Figure 5.11a**. As shown in **Figure**

**5.11b**, the linear range was observed in the concentration range from 0.02 to 0.18 μg/mL and correlation coefficient ($R^2$) 0.993.

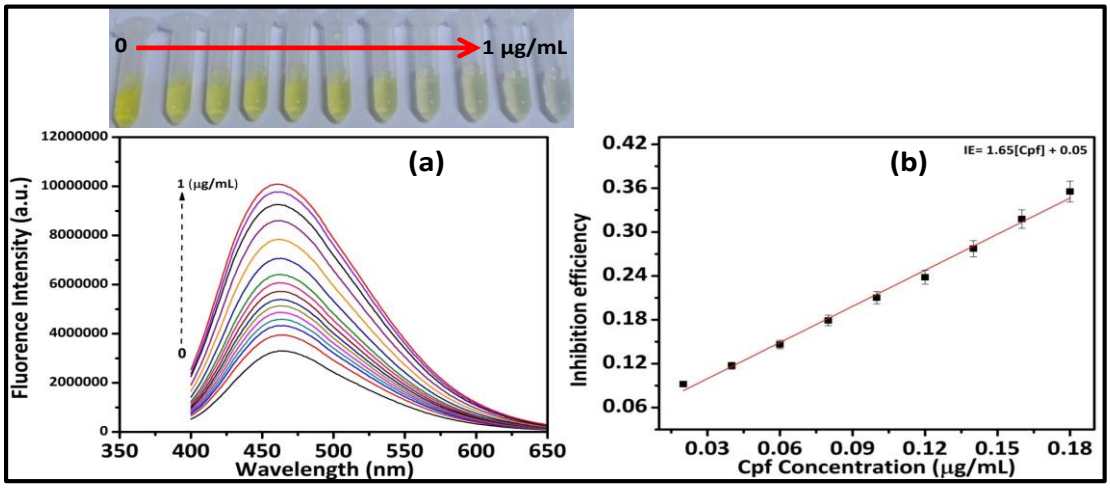


**Figure 5.11.** (a) Fluorescence emissions at 462 nm in the presence of various concentration of Cpf (0–1 μg/mL) in J-CQDs + DTNB + ATCh + AChE system, and also showing snap shot with increasing concentration from 0 to 1 μg/mL (b) Linear plot between IE and Cpf concentration (0.02–0.18 μg/mL).

The detection limit/ LOD of this optical process was calculated using 3σ rule by using the equation given in chapter 2 (equation 2.2)

The measured detection limit was 2.7 ng/mL, with signal to noise ratio of 3 (S/N=3), which is very low limit of detection compared to another published literature (**Table 5.1**). Therefore, the result indicates that the fluorescent detection of Cpf is simple, convenient and ultrasensitive.

**Table 5.1.** Comparison of different method with our synthesized nano-probe for the detection of Cpf.

| S.No. | Methods | Linear range | Limit of detection | Reference |
|---|---|---|---|---|
| 1. | Fluoroimmunoassay | - | 3.8 ng/mL | [Chen *et al.*(2010)] |
| 2. | Fluorescence-linked Immunosorbent method | 15.2–205.5 ng/mL | 8.4 ng/mL | [Chen *et al.* (2010)] |
| 3. | Fluorescence | 0.1–21.03 μg/m L | 5.9 ng/mL | [Ren *et al.* (2015)] |
| 4. | Quantum dot labeled molecularly imprinted Polymer | 20–200 ng/mL | 10 ng/mL | [Zhang *et al.* (2018)] |
| 5. | Immunochromatographic assay | - | 50 ng/mL | [Kim *et al.* (2011)] |
| 6. | Colorimetric | - | 50 ng/mL | [Guo *et al.* (2013)] |
| 7. | Fluorescence | 0.02 to 0.18 μg/mL | 2.7 ng/mL | This work |

Further, this proposed assay was not functional only for Cpf but also for other OPs. We explored the sensing platform for four conventional OPs including chlorpyrifos (Cpf), profenofos (Pro), malathion (Mal), and glyphosphate (Gly). The experimental processes were same as that for Cpf. As shown in **Figure 5.12**, we have evaluated inhibition efficiencies (IEs) of the above mentioned OPs such as 0.866, 0.610, 0.650, and 0.602 for Cpf, Pro, Mal, and Gly at the concentration of 0.2 μg/mL.

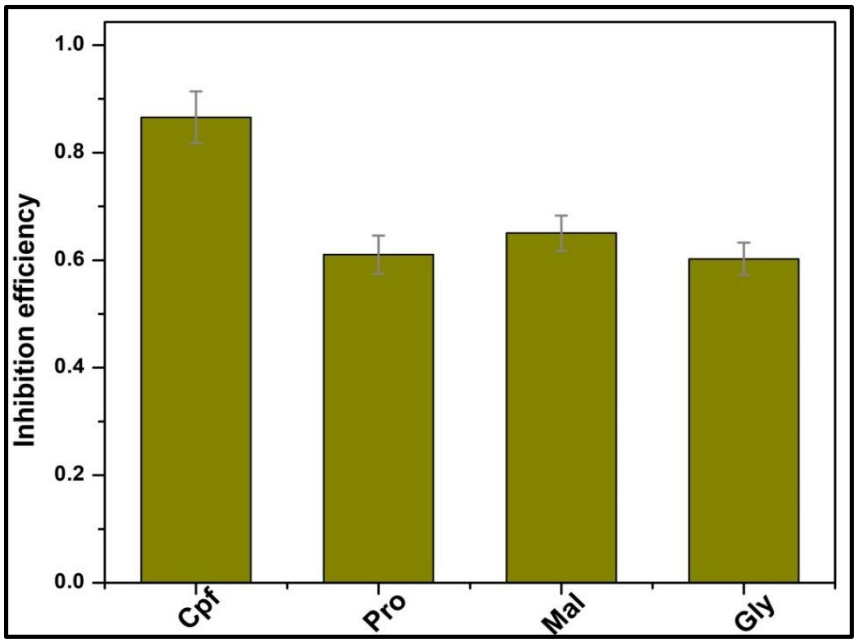


**Figure 5.12.** Inhibition efficiency (IE) of different OPs including chlorpyrifos (Cpf), profenofos (Pro), malathion (Mal), and glyphosphate (Gly), [OPs] = 0.2 μg/mL.

### 5.3.5. Selectivity of chlorpyrifos

Besides the sensitivity, selectivity is also an important sensing parameter to assess the sensing performance. Selectivity of the designed sensing system was checked over several metal ions, biomolecules and Cpf, which may be present in trace in environment and agricultural samples. The metal ions ($Fe^{2+}$, $Fe^{3+}$, $Na^{+}$, $K^{+}$, $Mg^{2+}$), glucose (Glu), lactose (Lac), ascorbic Acid (AA), uric Acid (UA), histidine (His), threonine (Thr), tryptophan (Try) of concentration 4 μg/mL (100 μL) and Cpf concentration 0.2 μg/mL (100 μL) were added into J-CQDs + ATCh + ATChE + DTNB system. A noticeable fluorescence change was observed in the presence of Cpf, while others had insignificant changes, as shown in **Figure 5.13a**. Interference of the planned sensing system was further explored in the system of J-CQDs + ATCh + ATChE + DTNB + Cpf. No perceptible change was observed in the fluorescence emission of J-CQDs after the addition of 100 μL (4 μg/mL) of these coexisting

molecules, as shown in **Figure 5.1.3b.** Thus, the substances did not exert any interference on the designed sensing system of Cpf.

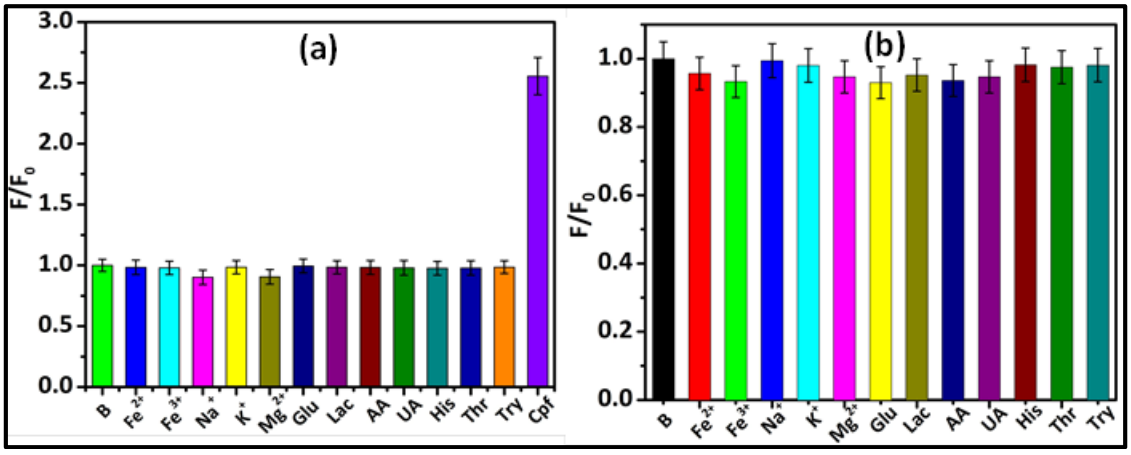


**Figure 5.13** (a) Represents the selectivity among different metal ions and various other amino acids (100 µL, 4 µg/mL), biomolecules (100 µL, 4 µg/mL) and cpf (100 µL, 0.2 µg/mL) in sensing system of J-CQDs + ATCh + ATChE + DTNB (b) Interference study of different metal ions (100 µL, 4 µg/mL) in J-CQDs + ATCh + ATChE + DTNB+Cpf system and various other molecules in the presence of Cpf (100 µL, 0.2 µg/mL).

### 5.3.6. Possible Mechanism

The fluorescence quenching mechanism for the detection of Cpf is based on the reaction of J-CQDs with TNBA. The designed sensor was based on the AChE, which catalyzed the ATCh into TCh. Furthermore, the TCh reacted with DTNB to form TNBA, which quenched the fluorescence intensity of J-CQDs. The existence of quenching procedure between J-CQDs and TNBA was established by the addition of different concentration of TNBA into J-CQDs. The fluorescence intensity of J-CQDs gradually decreased at 462 nm at excitation 370 nm with the increased concentration of TNBA from 0–10 µg/mL, as shown in **Figure 5.14a**. This result confirmed that there may be electrostatic interaction between J-CQDs and TNBA. To further confirm the quenching mechanism, the zeta potential of J-CQDs was analyzed before and after the addition of TNBA, as shown in **Figure 5.15**. In the presence of TNBA, the zeta potential of J-CQDs was reduced to -14.4 mV from -22.2 mV,

which confirmed the strong electrostatic interaction between J-CQDs and TNBA. Furthermore, to explore the quenching mechanism time resolve fluorescence spectra of J-CQDs were analyzed before and after addition of TNBA, as shown in **Figure 5.1.4b**. The fluorescence lifetime of J-CQDs was reduced to 3.12 ns from 4.54 ns, which confirmed the dynamic quenching process occurring via interaction between J-CQDs and TNBA.

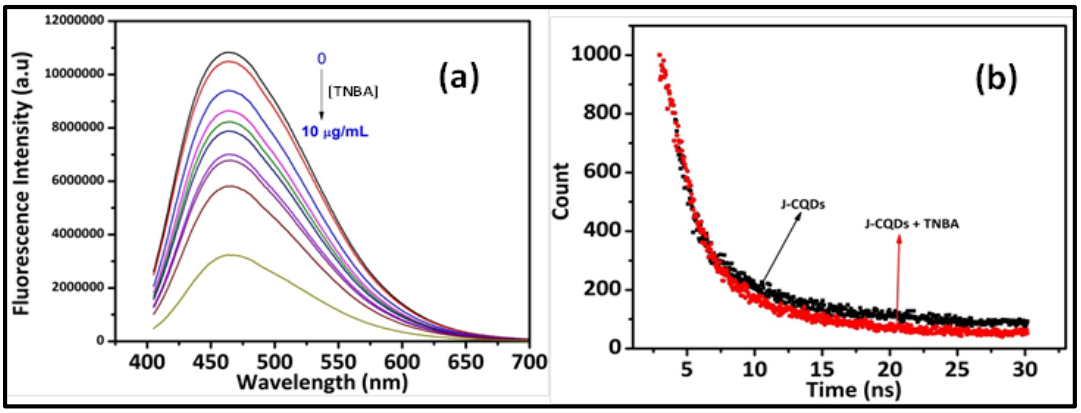


**Figure 5.14. (a)** Represents the emission spectra of J-CQDs on increasing the concentration of TNBA (b) Shows the fluorescence time resolved spectra of J-CQDs before and after addition of TNBA.

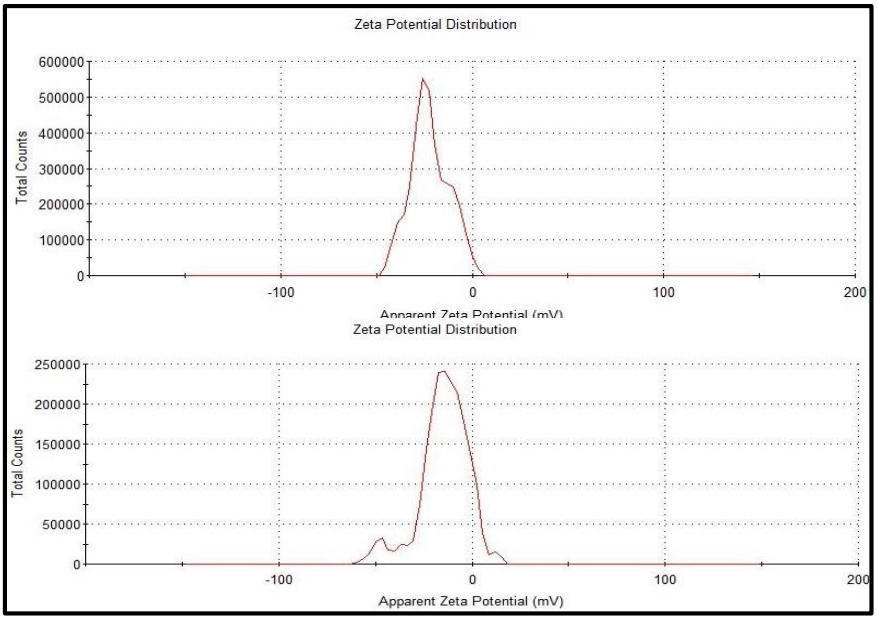


**Figure 5.15.** Zeta potential of the synthesized J-CQDs and TNBA.

Furthermore, the dynamic quenching may occur when excited state of J-CQDs return to ground state through energy or charge transfer process when impinged by TNBA molecule [M.J. Molaei *et al.* (2020)]. Additionally the unchanged absorbance spectra of J-CQDs upon interaction with TNBA moiety **(Figure 5.16)** support in claim for the occurrence dynamic quenching process [S. Kumar Panigrahi *et al.* (2019)]. Actually for dynamic quenching to be occurred there should be change or alteration in the absorption spectra of quantum dots in presence of analyte. But in the present case when UV-Visible absorption of J-CQDs in combination with TNBA analyte recorded, the spectra only reflected peaks corresponding to individual absorption of J-CQDs and TNBA recorded earlier. Indeed the spectral absorbance of J-CQDs + TNBA is nothing but mere superposition of individual absorbance spectra of J-CQDs and TNBA.

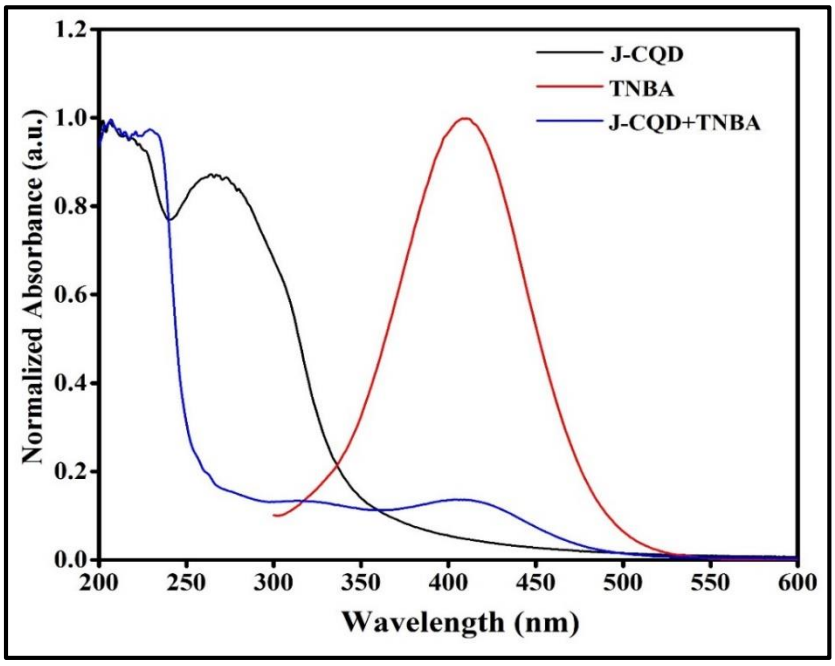


**Figure 5.16.** Absorbance spectra of J-CQDs, TNBA and J-CQDs and TNBA mixture

This is clearly shown in figure S6. There is no formation of any additional peaks and changes in peak position as well. Overall there is no shift or deviation in the J-CQDs +

TNBA absorption spectra. Interestingly overlapping absorbance spectra of TNBA with the excitation and emission spectra of J-CQDs **(Figure 5.17)** can lead to fluorescence quenching of latter as claimed by researcher [S. Kumar Panigrahi *et al.* (2019)]. However utmost care has been taken for delineating the inner filter effect by maintaining the J-CQDs concentration as low as possible. Generally, inner filter effect which is one of the major causes of fluorescence quenching, significantly boosted by concentration of fluorescent material during optical experiment. Hence in-order to delineate this effect during fluorescence measurement concentration of fluorophore is maintained as low as possible. Same procedure is adopted while measuring fluorescent intensity of J-CQDs, such that genuine cause of fluorescent quenching in combination with TNBA analyte could be postulated.

Moreover the altered excited state lifetime of fluorophore overruled the inner filter effect. The excitation/emission energy of J-CQDs not effectively re-absorbed by TNBA and thus could not masked fluorescent emission to display quenching effect.

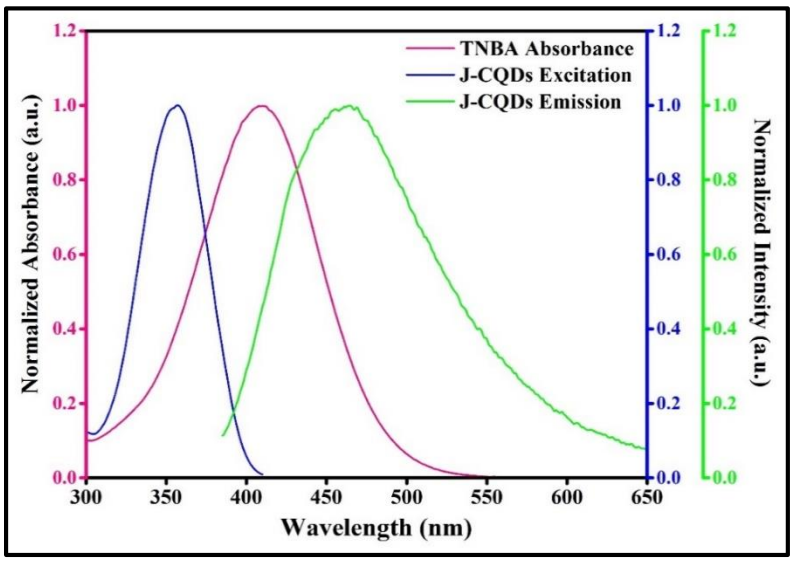


**Figure 5.17.** Overlapped absorbance spectra of TNBA on excitation and emission spectra of J-CQDs

## 5.4. Real Sample Analysis

In order to investigate the sensing feasibility, the designed system was applied on natural sample river water and apple juice. The river water sample was collected from the river Ganga, Varanasi, whereas apple juice was collected from the market. The experiments were performed with river water samples and apple juice spiked with the different concentration of Cpf (30, 50, 70 ng/mL). All the experiments were performed in triplicate. The sample recoveries were ranged from 93.3 to 102.0 %, and measured relative standard deviation (RSD) for n=3 were below 5%, as presented in **Table 5.2**. Moreover, the accuracy of our designed nanoprobe was further confirmed by Gas Chromatography (GC), which showed the good consistency to our experimental results. Thus, the proposed analysis showed the excellent accuracy and good recovery, which confirms that the J-CQDs based sensor exhibited an outstanding feasibility and reliability for the pesticides sensing in real samples.

**Table 5.2** Recovery experiment for the detection of Cpf into natural samples

| Samples | Before Spiking | Spiked Cpf (ng/mL) | Found (ng/mL) | | Recovery (%) | RSD (%) (n=3) |
|---|---|---|---|---|---|---|
| | | | Our method | GC | | |
| River water | 0 | 30 | 29.0 | 29.1 | 96.6 | 4.3 |
| | | 50 | 51.0 | 49.6 | 102.0 | 4.2 |
| | | 70 | 71.0 | 69.9 | 101.4 | 3.4 |
| Apple Juice | 0 | 30 | 28.0 | 28.8 | 93.3 | 2.9 |
| | | 50 | 48.0 | 47.3 | 96.0 | 1.7 |
| | | 70 | 68.0 | 69.4 | 97.1 | 4.1 |

## 5.5. Conclusion

In precise, we have fruitfully synthesized J-CQDs from the fruits of Jatropha. The J-CQDs showed excellent optical properties along with excellent quantum yield. Apart from this, the synthesized J-CQDs were utilized as a fluorescence nano-probe for the detection of

Cpf based on catalytic activity of AChE with good detection limit. The proposed sensing system was successfully applied on natural samples with good recovery efficiency. Therefore, the suggested method is scalable for analytical applications in food security and environmental monitoring fields and will provide favorable solutions for investigating of pesticide residues.